ISSN 1674-1056
http://cpb.iphy.ac.cn
http://iopscience.iop.org/cpb
中国物理 B
Chinese Physics
中国物理
Chinese Physics B

Effect of the potential function and strain rate on mechanical behavior of the single crystal Ni-based alloys: A molecular dynamics study

Qian Yin(尹倩), Ye-Da Lian(连业达), Rong-Hai Wu(巫荣海), Li-Qiang Gao(高利强), Shu-Qun Chen(陈树群), and Zhi-Xun Wen(温志勋)

Citation: Chin. Phys. B, 2021, 30 (**8**): 080204. DOI: 10.1088/1674-1056/abff22
Journal homepage: http://cpb.iphy.ac.cn; http://iopscience.iop.org/cpb

What follows is a list of articles you may be interested in

Atomistic simulations of the lubricative mechanism of a nano-alkane lubricating film between two layers of Cu-Zn alloy

Jing Li(李京), Peng Zhu(朱鹏), Yuan-Yuan Sheng(盛圆圆), Lin Liu(刘麟), and Yong Luo(罗勇)
Chin. Phys. B, 2021, 30 (**8**): 080205. DOI: 10.1088/1674-1056/abfbd6

Growth mode of helium crystal near dislocations in titanium

Bao-Ling Zhang(张宝玲), Bao-Wen Wang(王保文), Xue Su(苏雪), Xiao-Yong Song(宋小勇), Min Li(李敏)
Chin. Phys. B, 2018, 27 (**6**): 060205. DOI: 10.1088/1674-1056/27/6/060205

Temperature dependence of migration features of self-interstitials in zirconium

Rui Zhong(钟睿), Qing Hou(侯氢), Chao-Qiong Ma(马超琼), Bao-Qin Fu(付宝勤), Jun Wang(汪俊)
Chin. Phys. B, 2017, 26 (**12**): 120202. DOI: 10.1088/1674-1056/26/12/120202

Topology optimization using the improved element-free Galerkin method for elasticity

Yi Wu(吴意), Yong-Qi Ma(马永其), Wei Feng(冯伟), Yu-Min Cheng(程玉民)
Chin. Phys. B, 2017, 26 (**8**): 080203. DOI: 10.1088/1674-1056/26/8/080203

Brownian ratchet mechanism of translocation in T7 RNA polymerase facilitated by a post-translocation energy bias arising from the conformational change of the enzyme

Zhan-Feng Wang(王展峰), Zhi-Qiang Zhang(张志强), Yi-Ben Fu(付一本), Peng-Ye Wang(王鹏业), Ping Xie(谢平)
Chin. Phys. B, 2017, 26 (**3**): 030201. DOI: 10.1088/1674-1056/26/3/030201

Effect of the potential function and strain rate on mechanical behavior of the single crystal Ni-based alloys: A molecular dynamics study*

Qian Yin(尹倩)[1], Ye-Da Lian(连业达)[1,†], Rong-Hai Wu(巫荣海)[1,‡], Li-Qiang Gao(高利强)[1], Shu-Qun Chen(陈树群)[2], and Zhi-Xun Wen(温志勋)[1]

[1] *School of Mechanics, Civil Engineering and Architecture, Northwestern Polytechnical University, Xi'an* 710129, *China*
[2] *Key Laboratory of Advanced Functional Materials, Education Ministry of China, Beijing University of Technology, Beijing* 100124, *China*

(Received 5 March 2021; revised manuscript received ; accepted manuscript online 8 May 2021)

Molecular dynamics has been widely used to study the fundamental mechanism of Ni-based superalloys. However, the effect of the potential function and strain rate on mechanical behavior has rarely been mentioned in the previous molecular dynamics studies. In the present work, we show that the potential function of molecular dynamics can dramatically influence the simulation results of single crystal Ni-based superalloys. The microstructure and mechanical behavior of single crystal Ni-based superalloys under four commonly used potential functions are systematically compared. A most suitable potential function for the mechanical deformation is critically selected, and based on it, the role of strain rate on the mechanical deformation is investigated.

Keywords: defects, intermetallic alloys and compounds, microstructure, simulation and modeling

PACS: 02.70.Ns, 61.50.–f, 61.72.Nn, 61.72.Lk **DOI:** 10.1088/1674-1056/abff22

1. Introduction

Molecular dynamics (MD), as a means of explaining mechanism, has been used in the study of various materials.[1–7] For single crystal nickel-based superalloys, which are widely used as aero-engine hot-end components,[8–11] their microstructures mainly consist of matrix phase (or Ni phase) and precipitation phase (or Ni_3Al phase). A large number of researchers have used the MD method to study dislocation behaviors in Ni-based alloys.[12–20] Amodeo *et al.*[21] studied the deformation behavior of Ni_3Al under uniaxial compression and some researchers[22,23] studied the nanoindentation of nickel-containing structures. How to further study the mechanical properties of single crystal nickel-based superalloys by MD method was reviewed and prospected by Wu *et al.*[24] However, most of these simulation studies directly chose the potential functions, and there was no systematic comparison to indicate which is more reasonable. The effect of the strain rate on compression performance was also rarely studied. In this paper, several common potential functions will be selected to observe the different structural evolution and the compression process of different strain rates will be simulated under the most suitable potential function selected.

2. Simulation method

In this study, we performed the molecular dynamics simulation by using the LAMMPS software.[25] The dump files generated from LAMMPS were post-processed via the software of OVITO.[26] The atomic structure was analyzed by calculating the value of the centrosymmetry parameter.[27] The dislocations were identified by the dislocation extraction algorithm in the OVITO. During the compression simulation of Ni_3Al, a 10.0044 nm × 10.0044 nm × 10.0044 nm cubic model with a total of 87808 atoms was established and the periodic boundary condition was used. The lattice constant of Ni_3Al is 0.3573 nm. The NPT ensemble was used for equilibration, and the NVT ensemble was used for compression. The temperature of the whole simulation process was 300 K.

3. Results and discussion

3.1. The effect of potential function on mechanical deformation

We compare the microstructures and mechanical properties of the Ni_3Al under four commonly used potential functions, which include the Ni-Al-02, Ni-Al-09, Ni-Al-H, and Ni-Al-Re. The Ni-Al-02 potential[28] is generated by the fitting experimental data of B2-NiAl, L12-Ni_3Al, pure Ni, and

*Project supported by National Science and Technology Major Project of China (Grant No. 2017-IV-0003-0040), Fundamental Research Funds for the Central Universities in NWPU, China (Grant No. 31020180QD088), the National Natural Science Foundation of China (Grant Nos. 12002275 and 51904015), the Natural Science Foundation of Shaanxi Province, China (Grant No. 2020JQ-125), and General Program of Science and Technology Development Project of Beijing Municipal Education Commission, China (Grant No. KM202010005008).

†Corresponding author. E-mail: lianyeda@nwpu.edu.cn
‡Corresponding author. E-mail: ronghai.wu@nwpu.edu.cn

pure Al at different temperatures. The fitting data include equilibrium lattice parameter a_0, cohesive energy E_0, elastic constant, linear thermal expansion coefficient, and so on. The Ni-Al-09 potential,[29] based on functions for pure Ni and pure Al, is produced by fitting the experimental values of elastic constants, formation energy, and lattice parameter of NiAl. It can be used for simulations that do not involve the formation of structural vacancies, otherwise, the Ni-Al-02 potential would be a better choice. For the Ni-Al-H potential,[30] the interactions between atoms are determined by fitting properties such as vacancy formation energy, elastic constants, stacking fault energy for Ni–Ni, and partial molar volume, solution energy, migration energy for Ni–H. Several dislocations and grain boundaries in nickel were studied, and the interaction between hydrogen and various lattice defects in nickel was studied. This potential will soon be used to study the interaction between dislocations and precipitates in nickel. For the Ni-Al-Re potential,[31] monoatomic potentials are fitted to experimental properties and the pair potential is fitted to Ni_3Al properties and first-principles calculation results. It is accurately fitted to the basic lattice properties of pure Ni, Al, Re and Ni_3Al. The point defects, plane defects, and lattice misfit of γ and γ' are studied.

The MD simulation results of Ni_3Al structure with different potential functions during compression are shown in Fig. 1, where the green, blue, and red atoms represent the FCC, BCC, and HCP structures, respectively. The initial conditions of the four simulations are all the FCC Ni_3Al. When the potential is Ni-Al-02 (see Fig. 1(a)), the HCP atomic layers appear on the $\{111\}$ planes, which act as stacking faults in the original FCC structure. Simultaneously, the BCC atoms concentrate at the junctions of two HCP layers (see Fig. 1(a) at $\varepsilon = 0.175$). As the deformation goes on, the atomic layers of HCP expand continuously, and the atoms of FCC and BCC reduce. In the end, most of the atoms are transformed into HCP structure (see Fig. 1(a) at $\varepsilon = 0.25$). When using the Ni-Al-09 potential (see Fig. 1(b)) to compress, the BCC atoms first appear in the FCC structure, then gradually become dominant, and the remaining FCC atoms are mainly concentrated on the $\{110\}$ planes as stacking faults of the new BCC structure (see Fig. 1(b) at $\varepsilon = 0.175$). After that, the FCC atoms gradually disappear and all of them are transformed into BCC atoms (see Fig. 1(b) at $\varepsilon = 0.25$). When the Ni-Al-H potential function is used to simulate the compression (see Fig. 1(c)), the final microstructure is similar to that of Ni-Al-09. However, the intermediate microstructures of Ni-Al-H and Ni-Al-09 are distinct: The remaining FCC atoms of Ni-Al-H distribute randomly in the new BCC structure. When the Ni-Al-Re potential is used to simulate the Ni_3Al compression (see Fig. 1(d)), the microstructure evolution is similar to that of Ni-Al-02, except that the final microstructure of Ni-Al-Re is BCC instead of HCP. Twins are formed during the deformation. Only in the case of the Ni-Al-02 potential, the structure eventually transforms to the HCP dense structure, which is also the reason that assumed Ni-Al-02 is more suitable for compression.

The stress–strain curves under four potential functions are different, as shown in Fig. 2(a). The stress–strain curve of Ni-Al-02 first increases linearly then decreases in a zigzag form after $\varepsilon = 0.15$ and increases linearly again after $\varepsilon = 0.23$. By revisiting the microstructure evolution of Ni-Al-02 in Fig. 1(a), we can understand that the first linear increment of the stress–strain curve is due to the elastic deformation of FCC Ni_3Al, the following decrement is because of the formation of HCP stacking faults, and the final increment implies the elastic deformation of the well-formed HCP Ni_3Al. The shapes of the stress–strain curves of Ni-Al-09 and Ni-Al-Re are similar to that of Ni-Al-02. However, the stresses of Ni-Al-09 and Ni-Al-Re vanish at the end of the decrement stages, which are unreasonable. The shape of the stress–strain curve of Ni-Al-H is different from the rest three. An obvious difference is that instead of increasing linearly, the stress of Ni-Al-H decreases linearly in the final stage, which seems to contradict its microstructure evolution. Hence, it is reasonable to deduce that the Ni-Al-02 is the most suitable potential function for the mechanical deformation of single crystal Ni-based superalloys. It would be interesting to further investigate the mechanical features under the Ni-Al-02 potential function and understand more mechanisms. The evolution of crystal structure is shown in Fig. 2(b), which provides the quantitative fraction alteration of Fig. 1(a). Before $\varepsilon = 0.2$, the FCC dominates and the HCP acts as stacking faults. As stacking faults are constantly accomplished by partial dislocations as the edges of the stacking faults, the $\frac{1}{6}\langle 112\rangle$ Shockley partial dislocations are present as the only dislocation mechanism (see Fig. 2(c)). After $\varepsilon = 0.2$, the HCP dominates and the FCC acts as stacking faults with mainly $\frac{1}{3}\langle 001\rangle$ Hirth partial dislocations. Before the strain reaches 0.225, the dislocation is mainly Hirth dislocation, located at the edge of the faults. When the strain reaches 0.225, the dislocations disappear, because at this time the structure has changed into a dense HCP structure basically without stacking fault. Although the dislocation disappears, the structure becomes denser, and the atomic stress accumulates as the deformation increases. In the region with obvious stress fluctuations, the corresponding dislocation density is not zero, which indicates the stacking faults expansion and structural transformation.

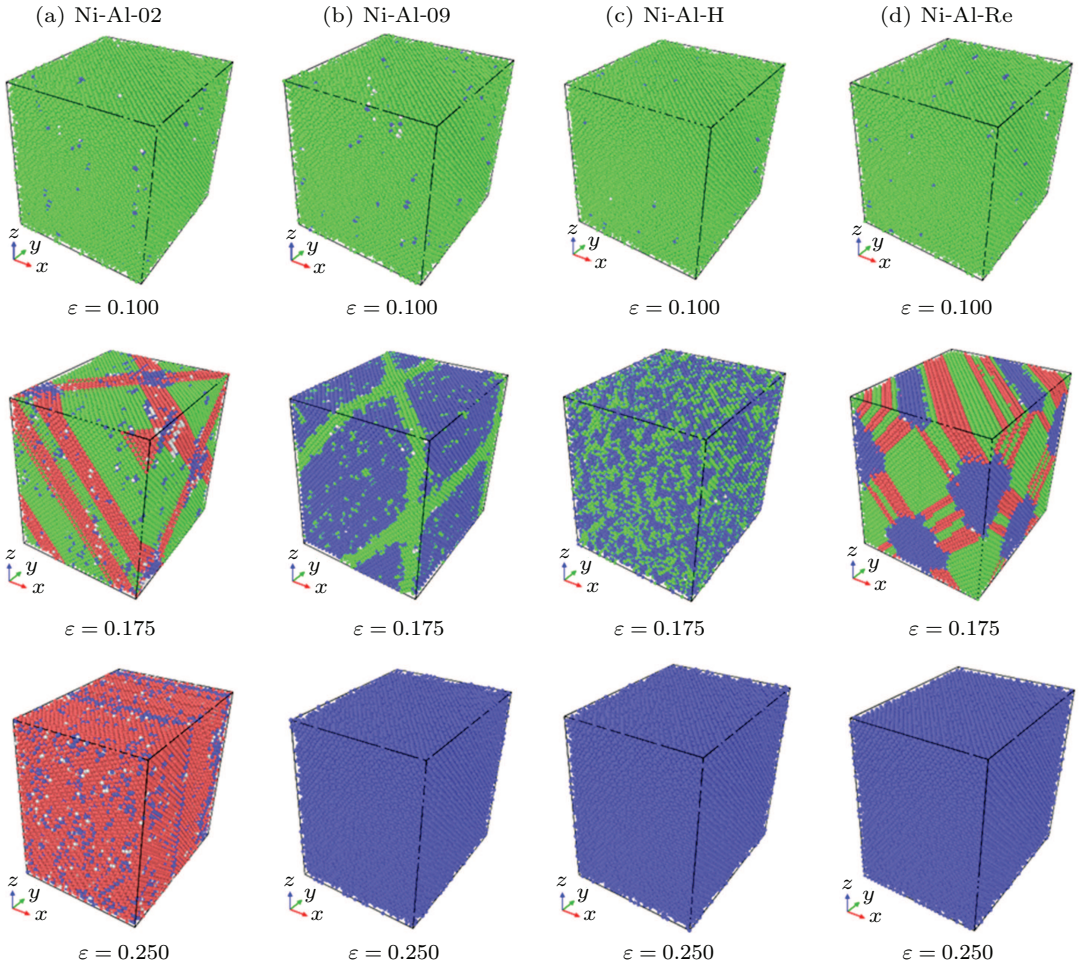

Fig. 1. The evolution of Ni_3Al structure under different potential functions during compression: (a) Ni-Al-02, (b) Ni-Al-09, (c) Ni-Al-H, (d) Ni-Al-Re. The green, blue, and red atoms are in the FCC, BCC, and HCP structures, respectively.

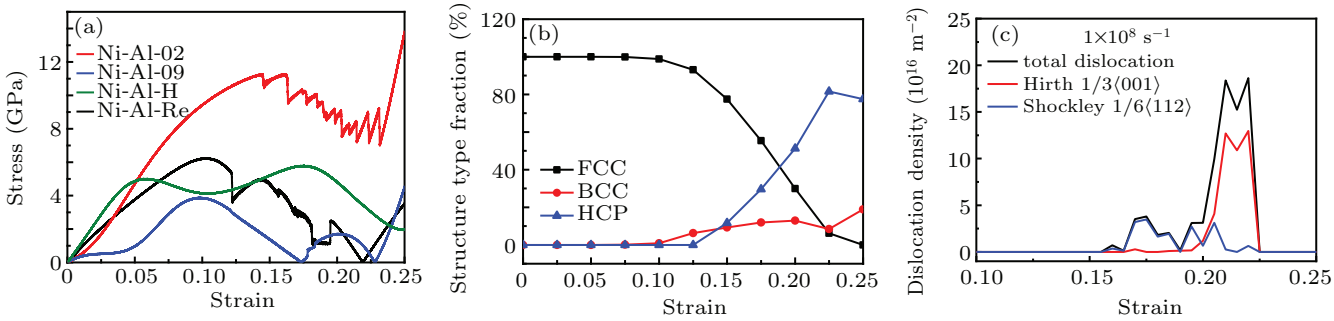

Fig. 2. (a) Stress–strain curves under four potential functions. (b) Evolution of crystal structure of the Ni-Al-02. (c) Evolution of dislocation density of the Ni-Al-02.

3.2. Compress simulation of Ni_3Al under different strain rates

At different strain rates during Ni_3Al compression, the structural changes are similar to those in Fig. 1(a), and the stress–strain curves and dislocation density are shown in Fig. 3. In the compression process of all strain rates, it is always FCC structure before the strain reaching 0.1. When the strain is between 0.1 and 0.145, BCC atoms are presented in the face-centered cubic structure and increase with the strain gradually, and no dislocations appear in this progress. When the strain reaches about 0.15, the HCP structure which belongs to the stacking fault area appears in the FCC structure, mainly located in the $\{111\}$ plane. At 5×10^7 s^{-1}, 1×10^8 s^{-1}, and 5×10^8 s^{-1} strain rates, stacking fault planes are mainly (111) and $(\bar{1}1\bar{1})$, and at 1×10^9 s^{-1} are $(\bar{1}1\bar{1})$ and $(1\bar{1}\bar{1})$. As the compression continues, the stacking fault expands continuously, and when the strain reaches 0.25, most of the atoms are converted to HCP structures. The model is in the elastic stage during the early compression process with the perfect FCC structure, so the dislocation density is zero. As the compression progresses, the FCC structure gradually transforms into BCC and HCP structures and begins to enter plastic deformation,

resulting in the dislocation nucleation. In the plastic stage, the dislocations react with each other, such as proliferation and annihilation. Meanwhile, the stacking fault expands and the structure transforms, resulting in the fluctuation of the dislocation density. Since the dislocation is mainly located at the edge of the stacking fault, when the structure is completely transformed from FCC to BCC or HCP, the fault disappears and the dislocation decreases to zero. Due to the different strain rates, the time of dislocation nucleation is different. The above explained the dislocation density evolution as shown in Figs. 2(c) and 3(b)–3(d). By comparing the stress–strain curves under different strain rates, it is found that the strain rate has almost no effect on the elastic deformation of the compression process, but only leads to different stress after forming stacking faults. The larger the strain rate is, the larger the corresponding strain will be when the dislocations occur. However, the overall change trend is similar, and the structural evolution is also similar. The production of Shockley dislocation leads to plastic deformation.

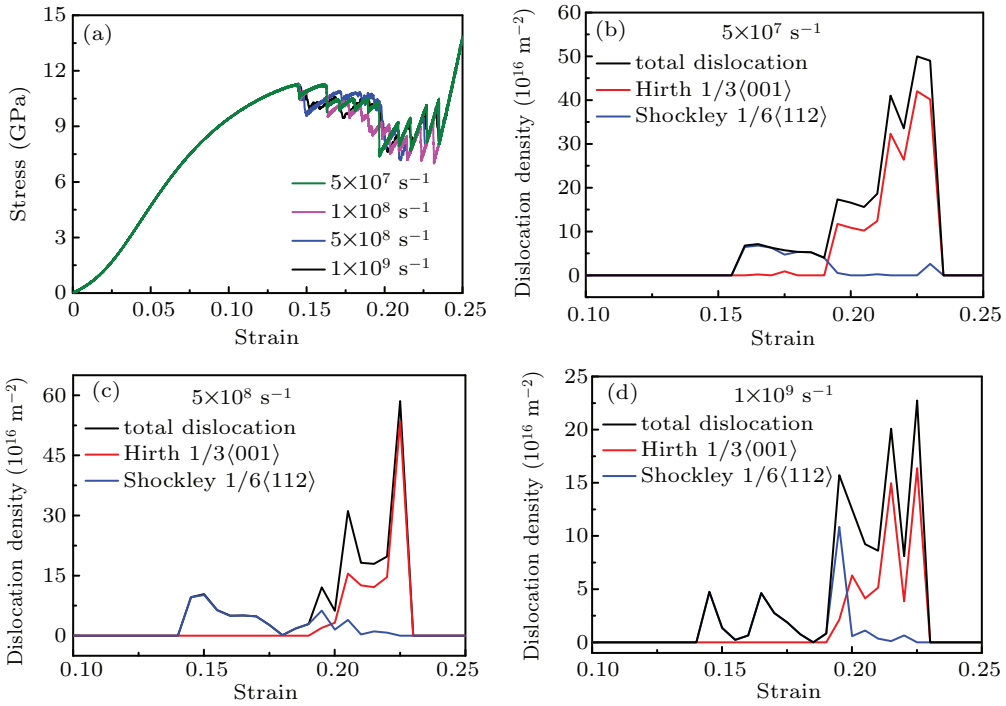

Fig. 3. (a) The stress–strain curves at different strain rates during compression of Ni_3Al and dislocation density at (b) 5×10^7 s^{-1}; (c) 5×10^8 s^{-1}; (d) 1×10^9 s^{-1}

4. Conclusion

By molecular dynamics, the present work systematically compared the microstructures and mechanical properties of single crystal Ni-based superalloys under four commonly used potential functions (i.e., Ni-Al-02, Ni-Al-09, Ni-Al-H, Ni-Al-Re) and four different strain rates (i.e., 5×10^7 s^{-1}, 1×10^8 s^{-1}, 5×10^8 s^{-1}, 1×10^9 s^{-1}). The main findings can be concluded as follows.

(i) Different potential functions result in different microstructure features and mechanical properties. Among the four potential functions, the Ni-Al-02 brings the most reasonable results and should be used for mechanical MD simulations in the future.

(ii) During compressive deformation of the Ni-Al-02, the microstructure is dominated by FCC structure with HCP stacking faults and Shockley partial dislocations before strain up to 0.2 and then gradually switches to HCP dominated with BCC stacking faults and the Hirth partial dislocations.

(iii) The influence of the strain rate on the elastic deformation behavior and crystal structure evolution is trivial, whereas higher strain rate leads to earlier and more formation of partial dislocations.

References

[1] Tominaga J, Sumi S and Awano H 2020 *Appl. Phys. Express* **13** 075503
[2] Ko W S, Choi W S, Xu G L, Choi P P, Lkeda Y and Grabowski B 2021 *Acta Mater.* **202** 331
[3] Maekawa Y, Sasaoka K and Yamamoto T 2019 *Appl. Phys. Express* **12** 115001
[4] Bryukhanov I A 2020 *Int. J. Plasticity* **135** 102834
[5] Kunugi R, Nakagawa N and Watanabe T 2017 *Appl. Phys. Express* **10** 031501
[6] Gong W B, Geng H Y, Qu S X and Lu W B 2017 *Appl. Phys. Express* **10** 105001
[7] An M R, Su M J, Deng Q, Song H Y, Wang C and Shang Y 2020 *Chin. Phys. B* **29** 46201
[8] Wen Z X, Zhang Y M, Li Z W and Yue Z F 2018 *Aerosp. Sci. Technol.* **82** 119
[9] Wen Z X, Pei H Q, Yang H, Wu Y W and Yue Z F 2018 *Int. J. Fatigue* **111** 243
[10] Li L, He K, Sun S Y, Yang W Z, Yue Z F and Wan H 2020 *Tribol. Lett.* **68** 26

[11] Xia W S, Zhao X B, Yue L and Zhang Z 2020 *J. Mater. Sci. Technol.* **44** 76
[12] Yashiro K, Naito M, and Tomita Y 2002 *Int. J. Mech. Sci.* **44** 1845
[13] Aihara T, Kaneko R and Kawazoe Y 2001 *Mater. Trans.* **42** 425
[14] Li Y L, Wu W P and Ruan Z G 2016 *Acta Metall. Sin.* **29** 1
[15] Li N L, Wu W P and Nie K 2018 *Phys. Lett. A* **382** 1361
[16] Chen B, Wu W P and Chen M X 2021 *Acta Mech. Solida Sin.* **34** 79
[17] Bitzek E, Brandl C, Derlet P M and Swygenhoven H V 2008 *Phys. Rev. Lett.* **100** 235501
[18] Zhu T and Wang C Y 2005 *Phys. Rev. B* **72** 014111
[19] Rodary E, Rodney D, Proville L, Bréchet Y and Martin G 2004 *Phys. Rev. B* **70** 054111
[20] Wang J P, Liang J W, Wen Z X and Yue Z F 2019 *Comp. Mater. Sci.* **160** 245
[21] Amodeo J, Begau C and Bitzek E 2014 *Mater. Res. Lett.* **2** 140
[22] Reddy K V and Pal S 2018 *Mol. Simulat.* **44** 1393
[23] Chamani M, Farrahi G H and Movahhedy M R 2016 *Comp. Mater. Sci.* **112** 175
[24] Wu R H, Zhao Y S, Yin Q, Wang J P, Ai X and Wen Z X 2021 *J. Alloys Compd.* **855** 157355
[25] Plimpton S 1995 *J. Comput. Phys.* **117** 1
[26] Stukowski A 2010 *Modelling Simul. Mater. Sci. Eng.* **18** 085001
[27] Kelchner L 1998 *Phys. Rev. B* **58** 11085
[28] Mishin Y, Mehl M J and Papaconstantopoulos D A 2002 *Phys. Rev. B* **65** 224114
[29] Pun G P and Mishin Y 2009 *Philosophical Magazine* **89** 3245
[30] Angelo J E, Moody N R and Baskes M I 1995 *Modelling Simul. Mater. Sci. Eng.* **3** 289
[31] Du J P, Wang C Y and Yu T 2012 *Modelling Simul. Mater. Sci. Eng.* **21** 015007